Deterministic Raman crosstalk effects in amplified wavelength division multiplexing transmission

Quan M. Nguyen and Avner Peleg

Department of Mathematics, State University of New York at Buffalo, Buffalo, New York 14260, USA

Abstract

We study the deterministic effects of Raman-induced crosstalk in amplified wavelength division multiplexing (WDM) optical fiber transmission lines. We show that the dynamics of pulse amplitudes in an N-channel transmission system is described by an N-dimensional predator-prey model. We find the equilibrium states with non-zero amplitudes and prove their stability by obtaining the Lyapunov function. The stability is independent of the exact details of the approximation for the Raman gain curve. Furthermore, we investigate the impact of cross phase modulation and Raman self and cross frequency shifts on the dynamics and establish the stability of the equilibrium state with respect to these perturbations. Our results provide a quantitative explanation for the robustness of differential-phase-shift-keyed WDM transmission against Raman crosstalk effects.

PACS numbers: 42.65.Dr, 42.81.Dp, 42.81.-i

I. INTRODUCTION

One of the important nonlinear processes affecting pulse propagation in massive wavelength division multiplexing (WDM) optical fiber communication systems is due to interpulse Raman-induced crosstalk [1, 2]. In this process, which takes place during collisions between pulses from different frequency channels (interchannel collisions), energy is transferred from high-frequency pulses to low-frequency pulses. It is known that the magnitude of the Raman-induced energy exchange in a single interchannel collision is independent of the frequency difference between the channels. Consequently, the magnitude of the cumulative energy shifts for a given pulse grows with the square of the number of channels, a result that is valid for linear transmission [3–6], conventional soliton transmission [7–10], and strongly dispersion-managed (DM) soliton transmission [11]. Therefore, in a 100-channel system, for example, the Raman crosstalk effects can be larger by a factor of 2.5×10^3 compared with a two-channel system operating at the same bit rate per channel.

Early studies of Raman crosstalk in WDM transmission focused on the dependence of the energy shifts on the total number of channels [3], as well as on the impact of energy depletion [5] and group velocity dispersion [12, 13] on the dynamics. Later on attention turned to the combined effects of Raman crosstalk and bit-pattern randomness in the on-off-keying (OOK) transmission scheme, and it was found that the probability density function (PDF) of the pulse amplitudes is lognormal [4, 6, 10, 14–16]. This finding means that the nth normalized moments of the amplitude grow exponentially with both propagation distance and n^2. Furthermore, in several studies of conventional soliton transmission it was found that the dynamics of the frequency shift is strongly coupled to amplitude dynamics, and as a result, the nth normalized moments of the Raman-induced self and cross frequency shifts also grow exponentially with propagation distance and n^2 (see Refs. [17–19]). This intermittent dynamic behavior has important practical consequences, by leading to relatively high bit-error-rate (BER) values at intermediate and large propagation distances [17–19]. Raman crosstalk effects were also recently investigated in hut-skipped amplified WDM transmission [20, 21], in cable television overlay passive optical networks [22, 23], in optical code-division multiple-access transmission systems [24], and in conjunction with four-wave-mixing [25].

One of the ways to overcome the detrimental effects of Raman crosstalk on massive WDM transmission is by replacing the OOK scheme by alternative encoding schemes, which are

expected to be less susceptible to these effects. The differential phase shift keying (DPSK) scheme, in which all time slots are occupied and the information is encoded in the phase difference between adjacent pulses, is one of the promising encoding methods that have attracted much interest in recent years [26, 27]. In DPSK transmission the Raman-induced amplitude dynamics becomes (approximately) deterministic, and important questions arise regarding the character of this dynamics. One major question concerns the possibility to achieve a stable equilibrium state for the amplitudes in all channels. The study reported in Ref. [5] demonstrated that this is not possible in unamplified optical fiber lines. However, later experiments showed that the situation is quite different in amplified WDM transmission [28, 29]. More specifically, it was found that the introduction of amplification into the system significantly reduces the Raman-induced energy shifts. In the present paper we suggest a dynamical explanation for this important experimental observation. Moreover, we demonstrate the robustness of DPSK transmission against inter-pulse Raman crosstalk effects by showing that equilibrium states with non-zero amplitudes in all channels do exist, and by proving the stability of the equilibrium states.

In the present study we consider optical solitons as an example for the pulses carrying the information for the following reasons. First, as mentioned above, the Raman-induced energy exchange in pulse collisions is similar in linear transmission, conventional soliton transmission, and strongly DM soliton transmission. Second, propagation of conventional solitons through an optical fiber is described by the nonlinear Schrödinger (NLS) equation, which is an integrable model [30]. Due to the integrability of the model, and to the fact that optical solitons are stable stationary solutions of the NLS equation, the derivation of the model for the Raman-induced amplitude dynamics can be done in a rigorous manner. Third, conventional optical solitons have traditionally been considered as excellent candidates for information transmission in high-speed optical fiber lines and in all-optical networks [1]. Furthermore, state-of-the-art transmission experiments already use all-Raman distributed amplification [31–37], which is the most suitable amplification scheme for conventional solitons.

Since we consider transmission systems where the pulses in each frequency channel are well-separated, intrachannel four-wave-mixing (FWM) effects are negligible. In addition, we assume that loss is compensated by distributed Raman amplification. It is a well-known fact in soliton theory that in the absence of loss interchannel FWM products completely vanish

after the collisions, see Ref. [30] for theory and Refs. [7, 38] for numerical simulations with the NLS equation with and without delayed Raman response. We remark that even in systems employing lumped amplifiers (and non-overlapping pulses), interchannel FWM can be significantly reduced by dispersion-management. This is true both in the soliton regime [38] and in the linear regime [39]. In contrast, the energy shift in a single collision between two strongly DM solitons is given by an expression with exactly the same form as the expression obtained for conventional solitons [11], i.e., strong dispersion-management does not reduce Raman crosstalk.

In deriving the model for Raman-induced amplitude dynamics we fully take into account pulse walk-off. In addition, we assume that the pulse sequences in all frequency channels are deterministic and that the sequences are either infinitely long or are subject to periodic temporal boundary conditions. The first setup approximates long-haul transmission, while the second one corresponds to a closed fiber loop experiment. We also assume that the constant net gain/loss in each channel is determined by the difference between distributed amplifier gain and fiber loss. Notice that in this feature our model is fundamentally different from the model derived in Ref [5]. Indeed, since in the latter model all channels experience net loss, it does not support an equilibrium state with non-zero amplitudes in all channels. In contrast, in our model the net gain/loss of some channels is positive while for other channels it is negative, which is the underlying reason for the existence of equilibrium states with non-zero amplitudes in all channels.

Our model for the Raman crosstalk dynamics in an N-channel system consists of a system of N coupled nonlinear ordinary differential equations (ODEs) for the amplitudes in different channels. The system of coupled ODEs can be described in the jargon of population dynamics theory as an N-dimensional predator-prey model [40]. After obtaining the model we look for equilibrium states with non-zero amplitudes in all channels and establish their stability with respect to deviations of the initial amplitudes from the equilibrium values. We also investigate the dynamic behavior induced by such deviations. In actual optical fiber transmission systems pulse dynamics can be influenced by physical processes other than Raman crosstalk. It is therefore important to understand the manner in which these additional processes perturb the Raman-induced amplitude dynamics. In the present study we investigate the effects of three perturbations due to cross phase modulation (XPM), Raman self frequency shift (SFS), and Raman cross frequency shift (XFS). For each of

these physical processes we construct the perturbed model describing amplitude dynamics in an N-channel system and investigate the existence of equilibrium states with non-zero amplitudes in all channels. Furthermore, we study the stability of the equilibrium state and the typical dynamic behavior of the amplitudes in two-channel systems in the presence of each of the three perturbations.

The rest of the paper is organized as follows. In Section II A we derive the unperturbed model for Raman-induced amplitude dynamics in WDM systems with $2N+1$ channels, and in Section II B we find the equilibrium states of the model and investigate their stability. In Section II C we validate the predictions of Section II B by numerical simulations. The perturbed models with XPM, Raman SFS, and Raman XFS, are studied in Sections III A, III B, and III C, respectively, for two-channel systems. Section IV is reserved for conclusions. In Appendix A we obtain the perturbed models with XPM, Raman SFS, and Raman XFS in WDM transmission with $2N+1$ channels.

II. DYNAMICS OF DETERMINISTIC RAMAN CROSSTALK - UNPERTURBED MODEL

A. Derivation of the model

Propagation of short pulses of light through an optical fiber in the presence of delayed Raman response is described by the following perturbed NLS equation [1]:

$$i\partial_z\psi + \partial_t^2\psi + 2|\psi|^2\psi = -\epsilon_R\psi\partial_t|\psi|^2, \tag{1}$$

where ψ is proportional to the envelope of the electric field, z is propagation distance and t is time in the retarded reference frame. The term $-\epsilon_R\psi\partial_t|\psi|^2$ represents the first order approximation for the fiber's delayed Raman response [41] and ϵ_R is the Raman coefficient [42]. When $\epsilon_R = 0$, the single-soliton solution of Eq. (1) in a frequency channel β is given by

$$\psi_\beta(t,z) = \eta_\beta \frac{\exp(i\chi_\beta)}{\cosh(x_\beta)}, \tag{2}$$

where $x_\beta = \eta_\beta\,(t - y_\beta - 2\beta z)$, $\chi_\beta = \alpha_\beta + \beta(t-y_\beta) + \left(\eta_\beta^2 - \beta^2\right) z$, and η_β, α_β and y_β are the soliton amplitude, phase and position, respectively.

Let us describe the main Raman-induced effects on a single collision between a soliton from the jth frequency channel and a soliton from the kth frequency channel. We assume that $\epsilon_R \ll 1/|\beta_j - \beta_k| \lesssim 1$, which is the typical situation in many WDM transmission systems even for adjacent channels [38, 39]. Under this assumption one can show that the most important effect of delayed Raman response on the collision is an $O(\epsilon_R)$ change in the soliton amplitude [7–10, 15]

$$\Delta\eta_j = 2\epsilon_R f(|j-k|)\mathrm{sgn}(\beta_k - \beta_j)\eta_j\eta_k, \tag{3}$$

where the coupling constants $f(|j-k|)$ depend on the specific approximation for the Raman gain curve. Notice that due to the inclusion of the $f(|j-k|)$ factors, Eq. (3) does not rely on the triangular approximation for the Raman gain curve. If we adopt the triangular approximation, we obtain that $f(|j-k|) = 1$ for any j and k. The effects of the collision in order $\epsilon_R/|\beta_j - \beta_k|$ will be described in Section III, where we obtain the perturbed models for amplitude dynamics. Since $\epsilon_R \ll 1/|\beta_j - \beta_k| \lesssim 1$, effects of order ϵ_R^2 and higher will be neglected. In addition, third order dispersion and self-steepening are neglected since the collision-induced effects of these conservative perturbations on the soliton amplitude and frequency are of higher order in both the parameter ϵ characterizing the perturbative process and $1/|\beta|$ (see, e.g., Refs. [43–45]).

Consider now WDM transmission systems with $2N+1$ channels and frequency difference $\Delta\beta$ between adjacent channels. Our model, which takes into account pulse walk-off, is based on the following assumptions. (1) The soliton sequences in all channels are deterministic in the sense that all time slots are occupied and each soliton is located at the center of a time slot of width T. Furthermore, when considering amplitude dynamics, the amplitudes are equal for all pulses from the same frequency channel, but are not necessarily equal for pulses from different channels. This setup corresponds, for example, to return-to-zero (RZ) transmission with differential-phase-shift-keying [46]. (2) The sequences are either (a) infinitely long, or (b) subject to periodic temporal boundary conditions. Notice that setup (a) is an approximation for long-haul transmission systems, while setup (b) is an approximation for closed fiber-loop experiments. (3) The gain/loss in each channel is determined by the difference between distributed amplifier gain and fiber loss. In particular, for some channels this difference can be slightly positive, resulting in small net gain, while for other channels this difference can be slightly negative, resulting in small net loss. We emphasize that in

this feature our model is essentially different from the models that are usually considered in studies of Raman amplification schemes, where it is assumed that *all* pumps experience net loss [1, 5].

To obtain the dynamic equation for the amplitude of the jth-channel solitons we note that the distance traveled by these solitons while passing two successive solitons in the $j-1$ or $j+1$ channels is $\Delta z_c^{(1)} = T/(2\Delta\beta)$. We denote by z_l the location of the lth collision of a given jth-channel soliton with solitons in the $j+1$ or $j-1$ channel. Using Eq. (3) and summing over all collisions occurring within the interval $(z_{l-1}, z_l]$, where $z_l = z_{l-1} + \Delta z_c^{(1)}$, we obtain

$$\eta_j(z_{l-1} + \Delta z_c^{(1)}) = \eta_j(z_{l-1}) + g_j\eta_j(z_{l-1})\Delta z_c^{(1)} + 2\epsilon_R \sum_{k=-N}^{N} (k-j) f(|j-k|)\eta_j(z_{l-1})\eta_k(z_{l-1}). \quad (4)$$

The constant g_j on the right hand side of Eq. (4) is the net gain/loss coefficient for the jth channel, which is assumed to be independent of z. Due to the periodicity of the pulse sequences the same equation is satisfied by the amplitudes of all jth-channel solitons. Moreover, the same equations with different j values, where $j = -N, \ldots, N$, describe the dynamics of the soliton amplitudes in all channels. Going to the continuum limit we obtain

$$\frac{d\eta_j}{dz} = \eta_j \left[g_j + C \sum_{k=-N}^{N} (k-j) f(|j-k|)\eta_k \right], \quad (5)$$

where $C = 4\epsilon_R\Delta\beta/T$ and $j = -N, \ldots, N$. The system (5) gives a complete description of the dynamics of the η_j's. Notice that apart from the important fact that some gain/loss coefficients can be positive while others can be negative, the system (5) is similar to the one obtained in Ref. [5] for the Raman-induced amplitude dynamics of continuous waves in unamplified WDM transmission. Thus, our model also describes the Raman-induced crosstalk dynamics of continuous waves in amplified WDM transmission systems.

B. Equilibrium states, stability, and conserved quantities

In optical fiber communication systems it is usually desired to achieve a steady state in which the pulse amplitudes in all channels are equal and constant (independent of z) [1]. We therefore look for an equilibrium state of the system (5) in the form $\eta_j^{(eq)} = \eta > 0$ for

$-N \le j \le N$. Setting the right hand sides of (5) equal to zero we arrive at

$$g_j = -C\eta \sum_{k=-N}^{N} (k-j) f(|j-k|). \tag{6}$$

Therefore, the gain required to maintain an equilibrium state with equal amplitudes is *not* flat with respect to frequency. Instead, the net gain/loss coefficient of high-frequency channels should be positive, while that of low-frequency channels should be negative. In other words, high-frequency channels should be overamplified, whereas low-frequency channels should be underamplified compared with the reference ($j = 0$) channel. Substituting Eq. (6) into Eq. (5) we arrive at a slightly simpler form of the model, which is convenient for analysis and numerical simulations,

$$\frac{d\eta_j}{dz} = C\eta_j \sum_{k=-N}^{N} (k-j) f(|j-k|)(\eta_k - \eta). \tag{7}$$

Equation (7) can be described in population dynamics terminology as a predator-prey system with $2N+1$ species [40].

The equilibrium states of Eq. (7) with non-zero amplitudes are determined by

$$\sum_{k=-N}^{N} (k-j) f(|j-k|)(\eta_k^{(eq)} - \eta) = 0, \qquad -N \le j \le N. \tag{8}$$

The trivial solution of Eq. (8), that is, the solution with $\eta_k^{(eq)} = \eta > 0$ for $-N \le k \le N$, corresponds to the equilibrium state of Eq. (7) with equal non-zero amplitudes. However, due to the anti-symmetry of $(k-j)f(|j-k|)$ with respect to an interchange of j and k, Eq. (8) has infinitely many non-trivial solutions, and these correspond to equilibrium states of Eq. (7) with unequal non-zero amplitudes [47]. In the case where the Raman gain curve is described by the triangular approximation it is straightforward to show that the non-trivial equilibrium states of Eq. (7) are determined by the following two equations:

$$\sum_{k=-N}^{N} \eta_k^{(eq)} = (2N+1)\eta, \qquad \sum_{k=-N}^{N} k\eta_k^{(eq)} = 0. \tag{9}$$

Therefore, in this case the equilibrium states lie on a $(2N-1)$-dimensional plane. Thus, for a 3-channel system, for example, the equilibrium states lie on the line segment $(\eta, \eta, \eta) - (b-\eta)(1/2, -1, 1/2)$, where $0 < b < 3\eta$.

We now prove stability of all equilibrium states of Eq. (7) with non-zero amplitudes, $\eta_j = \eta_j^{(eq)} > 0, -N \leq j \leq N$, by constructing a Lyapunov function for this equation. For this purpose we consider the function

$$V_L(\boldsymbol{\eta}) = \sum_{j=-N}^{N} \left[\eta_j - \eta_j^{(eq)} + \eta_j^{(eq)} \ln \left(\frac{\eta_j^{(eq)}}{\eta_j} \right) \right], \tag{10}$$

where $\boldsymbol{\eta} = (\eta_{-N}, \ldots, \eta_j, \ldots, \eta_N)$. Taking the derivative of $V_L(\boldsymbol{\eta})$ along trajectories of the system (7) we obtain

$$\frac{dV_L}{dz} = \sum_{j=-N}^{N} \frac{\eta_j - \eta_j^{(eq)}}{\eta_j} \frac{d\eta_j}{dz} = C \sum_{j=-N}^{N} (\eta_j - \eta_j^{(eq)}) \sum_{k=-N}^{N} (k-j) f(|j-k|)(\eta_k - \eta). \tag{11}$$

From Eq. (8) it follows that $\sum_{k=-N}^{N}(k-j)f(|j-k|)(\eta_k - \eta) = \sum_{k=-N}^{N}(k-j)f(|j-k|)(\eta_k - \eta^{(eq)})$. Using this relation together with Eq. (11) and the anti-symmetry of $(k-j)f(|j-k|)$ we arrive at

$$\frac{dV_L}{dz} = \sum_{j=-N}^{N} \sum_{k=-N}^{N} (k-j) f(|j-k|)(\eta_j - \eta_j^{(eq)})(\eta_k - \eta^{(eq)}) = 0, \tag{12}$$

for $\eta_j > 0, -N \leq j \leq N$. It is straightforward to show that each term $h(\eta_j) = \eta_j - \eta_j^{(eq)} + \eta_j^{(eq)} \left[\ln(\eta_j^{(eq)}/\eta_j) \right]$ on the right hand side of Eq. (10) satisfies $h(\eta_j) \geq 0$ for any $\eta_j > 0$, where $h(\eta_j) = 0$ only at $\eta_j = \eta_j^{(eq)}$. Therefore, $V_L(\boldsymbol{\eta}) \geq 0$ for any vector $\boldsymbol{\eta}$ for which $\eta_j > 0$ for $-N \leq j \leq N$, where equality holds only at equilibrium points. Combining this result with the result $dV_L/dz = 0$ along trajectories of the system we conclude that V_L is a Lyapunov function of the system (7) and therefore the equilibrium states $\eta_j = \eta_j^{(eq)} > 0, -N \leq j \leq N$ are stable [48, 49]. We note that since $dV_L/dz = 0$ rather than $dV_L/dz < 0$ this stability means that the values of $\eta_j(z)$ are bounded for any z but do not tend to $\eta_j^{(eq)}$ for large propagation distance z. Thus, the typical dynamics of the amplitudes $\eta_j(z)$ for initial conditions that are off the equilibrium point is oscillatory. Notice that the stability is independent of the exact specification of the $f(|j-k|)$ values, and therefore the equilibrium states are stable irrespective of the specific details of the approximation for the Raman gain curve. Notice also that Eq. (10) actually provides $K+1$ independent conserved quantities for the model (7), where K is the dimension of the solution space of Eq. (8). For example, if the Raman gain is described by the triangular approximation, $K = 2N-1$, and there are $2N$ conserved quantities in total.

C. Numerical solution of the system (7)

In order to check the predictions of the previous subsection we solve Eq. (7) numerically by employing a fourth-order Runge-Kutta method. As a concrete example for the physical parameter values we consider a 101-channel system operating at 40 Gbits/s per channel with frequency spacing $\Delta\nu = 100$ GHz and dimensionless time slot width $T = 5$. With this choice the pulse width is 5 ps, $\Delta\beta = \pi$, $\epsilon_R = 0.0012$, and $N = 50$. These parameter values are typical for several state-of-the-art massive multichannel transmission experiments, see Ref. [39] and references therein. Taking $\beta_2 = -1\text{ps}^2\text{km}^{-1}$ and $\gamma = 4\text{W}^{-1}\text{km}^{-1}$ we obtain $P_0 = 10$ mW for the soliton peak power. The dimensionless final propagation distance is taken as $z_f = 200$ corresponding to $X_f = 10^4$ km, but the main features of the dynamics can already be observed at considerably shorter distances. We also choose $\eta = 1$, so that the trivial equilibrium state is $\eta_j^{(eq)} = 1$, for all j.

To illustrate the impact of Raman crosstalk on *massive* WDM transmission we focus attention on amplitude dynamics of solitons from faraway channels. Thus, we start by considering a two-channel system consisting of the reference channel ($j = 0$) and the highest-frequency channel $j = N = 50$. Employing Eq. (7) to this two-channel system while adopting the triangular approximation for the Raman gain curve we obtain

$$\begin{aligned} \frac{d\eta_{50}}{dz} &= 50C\eta_{50}\left(1-\eta_0\right), \\ \frac{d\eta_0}{dz} &= 50C\eta_0\left(\eta_{50}-1\right). \end{aligned} \tag{13}$$

The solution of Eq. (13) for $\eta_0 > 0$ and $\eta_1 > 0$ is

$$\eta_{50}(z) + \eta_0(z) - \ln\left[\eta_{50}(z)\right] - \ln\left[\eta_0(z)\right] = \kappa, \tag{14}$$

where the constant κ is determined by the values of $\eta_0(0)$ and $\eta_{50}(0)$. The z-dependence of the amplitudes η_0 and η_{50} is shown in Fig. 1 (a) for the initial condition $\eta_{50}(0) = 1.2$ and $\eta_0(0) = 0.9$. It is clearly seen that the amplitudes oscillate about their equilibrium value $\eta = 1$. The dimensionless oscillation period is $Z_p = 41.8$, corresponding to 2090 km [50]. Similar oscillatory behavior is observed for other choices of the initial amplitudes. Figure 1 (b) shows the phase portrait for the system (13). Since all trajectories are closed curves we conclude that the dynamics is indeed periodic and that the equilibrium state is stable.

Next we consider a three-channel system consisting of the channels $j = 0$ and $j = \pm 50$.

Within the Raman triangular approximation the amplitude dynamics is described by

$$\begin{aligned}
\frac{d\eta_{50}}{dz} &= 50C\eta_{50}\left(3-\eta_0-2\eta_{-50}\right), \\
\frac{d\eta_0}{dz} &= 50C\eta_0\left(\eta_{50}-\eta_{-50}\right), \\
\frac{d\eta_{-50}}{dz} &= 50C\eta_{-50}\left(-3+2\eta_{50}+\eta_0\right).
\end{aligned} \tag{15}$$

Figure 2 (a) shows the phase portrait. The solid line is the line segment of stable equilibrium points $(1,1,1)-(b-1)(1/2,-1,1/2)$, where $0<b<3$. Since all trajectories are closed orbits centered about the equilibrium line we conclude that the equilibrium states are indeed stable and that the amplitudes exhibit periodic oscillations. This oscillatory dynamics is illustrated in Fig. 2 (b) for the initial condition $\eta_{50}(0)=0.8$, $\eta_0(0)=0.9$, $\eta_{-50}(0)=1.1$.

As another example for possible dynamic scenarios exhibited by the unperturbed model (7) we study a four-channel system consisting of the channels $j=\pm 16$ and $j=\pm 48$. As we demonstrate below, a four-channel setup represents the simplest case where deviations from the triangular approximation for the Raman gain curve lead to the emergence of new dynamical features. We consider the following sets of values for the coupling constants $f(|j-k|)$: $f(1)=f(2)=1$ and $f(3)=1+p$, where $p=0$ for set (1) and $p=0.1$ for set (2). Thus, set (1) corresponds to the triangular approximation, whereas set (2) represents a 10% deviation from the triangular approximation for $f(3)$. For these values of the coupling constants the dynamics of the amplitude is described by

$$\begin{aligned}
\frac{d\eta_{48}}{dz} &= 32C\eta_{48}\left[(6+3p)-\eta_{16}-2\eta_{-16}-3(1+p)\eta_{-48}\right], \\
\frac{d\eta_{16}}{dz} &= 32C\eta_{16}\left(2+\eta_{48}-\eta_{-16}-2\eta_{-48}\right), \\
\frac{d\eta_{-16}}{dz} &= 32C\eta_{-16}\left(-2+2\eta_{48}+\eta_{16}-\eta_{-48}\right), \\
\frac{d\eta_{-48}}{dz} &= 32C\eta_{-48}\left[-(6+3p)+3(1+p)\eta_{48}+2\eta_{16}+\eta_{-16}\right].
\end{aligned} \tag{16}$$

We solve the system (16) numerically with $p=0$ and $p=0.1$ and with the initial condition $\eta_{48}(0)=1.2$, $\eta_{16}(0)=1.1$, $\eta_{-16}(0)=0.95$, and $\eta_{-48}(0)=0.9$. The results of our numerical simulations are presented in Figs. 3 and 4. As can be seen, in both cases the amplitudes exhibit oscillatory dynamics. However, in the triangular approximation case ($p=0$) there is only a single period for the oscillations, whereas in the non-triangular approximation case ($p=0.1$) two very different oscillation periods are observed. The first period is not

significantly different from the oscillation period for $p = 0$, while the second period is much longer than the first one (see Fig. 4). In fact, in order to verify that the amplitude dynamics is indeed periodic for $p = 0.1$ one has to carry out the simulation up to a final propagation distance of $z_f = 2000$.

Notice that our choice of 40 Gbits/s per channel systems is mainly for reasons of convenience, since with this value we can illustrate the oscillatory nature of the Raman-induced amplitude dynamics already with two and three channels. Since current soliton-based systems work at 10 Gbits/s per channel it is useful to examine one example for the amplitude dynamics in such systems. We therefore consider a 361-channel system operating at 10 Gbits/s per channel with frequency spacing $\Delta\nu = 25$ GHz and dimensionless time slot width $T = 5$. For these parameter values the pulse width is 20 ps, $\Delta\beta = \pi$, $\epsilon_R = 3 \times 10^{-4}$, and $N = 180$. Taking $\beta_2 = -2\text{ps}^2\text{km}^{-1}$ and $\gamma = 2\text{W}^{-1}\text{km}^{-1}$ we obtain $P_0 = 2.5$ mW for the soliton peak power. The dimensionless final propagation distance is taken as $z_f = 25$ corresponding to $X_f = 10^4$ km, but the main dynamical features can already be observed at shorter distances. As before we choose $\eta = 1$, so that the trivial equilibrium state is $\eta_j^{(eq)} = 1$, for all j. To illustrate the dynamics we consider a seven-channel system consisting of the channels $j = 0$, $j = \pm 60$, $j = \pm 120$, and $j = \pm 180$ and adopt the triangular approximation for the Raman gain curve. The corresponding system of equations for amplitude evolution is solved numerically with the initial condition $\eta_{180}(0) = 1.2$, $\eta_{120}(0) = 1.05$, $\eta_{60}(0) = 1.1$ $\eta_0(0) = 1.15$, $\eta_{-60}(0) = 0.98$, $\eta_{-120}(0) = 1.1$, and $\eta_{-180}(0) = 0.95$. The results are shown in Fig. 5. One can see that pulse amplitudes in all channels exhibit oscillatory behavior similar to the one observed in Figures 1 and 2 for the 40 Gbits/s per channel system. Thus, equilibrium states with non-zero amplitudes in all channels are stable in both 10 and 40 Gbits/s per channel systems, in agreement with the predictions in Section II B.

III. DYNAMICS OF DETERMINISTIC RAMAN CROSSTALK - PERTURBED MODELS

We now turn to study the effects of perturbations on the model described by Eq. (7). We focus attention on the effects of cross phase modulation (XPM), Raman self frequency shift (SFS), and Raman cross frequency shift (XFS). It is well-known that each of these processes by itself does not change the soliton amplitude. Thus, in the absence of Raman crosstalk the

soliton amplitudes are constant and there is no amplitude dynamics to be considered. As we show below XPM, Raman SFS, and Raman XFS affect amplitude dynamics by leading to z-dependence of the collision rate. For these reasons, the three processes can be considered as perturbations to the model (7). For each of the three processes we develop a perturbed model for amplitude dynamics and analyze the stability of the equilibrium state and the dynamic behavior in the new model. Here we choose to concentrate on a two-channel system consisting of channels $j = 0$ and $j = 1$ since such treatment is sufficient in order to uncover the main changes in the dynamics compared with the unperturbed model. Without loss of generality we assume $f(1) = 1$ for the coupling constant. The general forms of the perturbed models in WDM systems with $2N + 1$ channels are obtained in Appendix A.

A. Effects of cross phase modulation

The XPM-induced position shift experienced by a soliton in the jth channel as a result of a single collision with a kth-channel soliton is given by (see, e.g., Refs. [15, 38])

$$\Delta y_j = \frac{4\mathrm{sgn}(\beta_k - \beta_j)\eta_k}{(\beta_k - \beta_j)^2}. \tag{17}$$

Our goal is to obtain a perturbed model for the dynamics of the amplitudes η_0 and η_1 in the two-channel system, which takes into account the XPM-induced position shift. It is clear that the main effect of the position shift (17) is to lead to a change in the inter-collision distance $\Delta z_c^{(1)}$, that is, $\Delta z_c^{(1)}$ is z-dependent in the perturbed model. In order to find this z-dependence we first write down the equation for the location of the lth collision of the soliton from the zero time slot in the reference channel. Since this collision is with the soliton from the $-l$ time slot in channel 1, the collision distance z_l is determined by

$$y_{1,-l}(z_l) = y_{0,0}(z_l), \tag{18}$$

where the first subscript in $y_{1,-l}$ stands for the channel and the second subscript represents the time slot. Taking into account the difference in group velocities, $2\beta_1$, and the position shifts experienced by the solitons in the collision we find

$$y_{1,-l}(z_{l-1}) + 2\beta_1 \Delta z_c^{(1)}(z_{l-1}) - 4\eta_0(z_{l-1})/\beta_1^2 = y_{0,0}(z_{l-1}) + 4\eta_1(z_{l-1})/\beta_1^2. \tag{19}$$

Solving Eq. (19) for $\Delta z_c^{(1)}$ we obtain

$$\Delta z_c^{(1)}(z_{l-1}) = \frac{1}{2\beta_1}\left[y_{0,0}(z_{l-1}) - y_{1,-l}(z_{l-1})\right] + \frac{2}{\beta_1^3}\left[\eta_0(z_{l-1}) + \eta_1(z_{l-1})\right]. \tag{20}$$

From the definition of z_{l-1} and the periodicity of the pulse sequences it follows that $y_{0,0}(z_{l-1}) - y_{1,-l}(z_{l-1}) = T$. Therefore, Eq. (20) can be rewritten as

$$\Delta z_c^{(1)}(z_{l-1}) = \frac{T}{2\beta_1}\left\{1 + B\left[\eta_0(z_{l-1}) + \eta_1(z_{l-1})\right]\right\}, \tag{21}$$

where $B = 4/(T\beta_1^2)$. Notice that $\Delta z_c^{(1)}(z_{l-1}) > T/(2\beta_1)$ due to the fact that the XPM-induced position shifts are positive for the reference channel solitons and negative for the solitons in channel 1. The equations for the amplitudes η_0 and η_1 at $z_l = z_{l-1} + \Delta z_c^{(1)}(z_{l-1})$ are similar in form to Eq. (4). Substituting relation (21) into the equations for $\eta_0(z_{l-1} + \Delta z_c^{(1)})$ and $\eta_1(z_{l-1} + \Delta z_c^{(1)})$ and going to the continuum limit we obtain

$$\begin{aligned}
\frac{d\eta_1}{dz} &= \eta_1\left[g_1 - \frac{C\eta_0}{1 + B\left(\eta_0 + \eta_1\right)}\right], \\
\frac{d\eta_0}{dz} &= \eta_0\left[g_0 + \frac{C\eta_1}{1 + B\left(\eta_0 + \eta_1\right)}\right].
\end{aligned} \tag{22}$$

Equation (22) represents the perturbed model that takes into account XPM effects. Notice that for the typical values $T = 5$ and $\beta_1 = \pi$, $B \simeq 0.081$, i.e., $B \ll 1$. Thus, for such values the XPM perturbation can be considered as a weak perturbation.

We look for equilibrium states of Eq. (22) that are of the form $\eta_0^{(eq)} = \eta_1^{(eq)} = \eta > 0$. This requirement yields the expressions $g_1 = -g_0 = C\eta/(1 + 2B\eta)$ for the gain/loss coefficients. Thus, an important consequence of the XPM-induced position shifts is a change in the values of the gain/loss coefficients that are required for maintaining an equilibrium state with equal non-zero amplitudes. Taking into account the modified expressions for g_0 and g_1, we can rewrite Eq. (22) as

$$\begin{aligned}
\frac{d\eta_1}{dz} &= C\eta_1\left[\frac{\eta}{1 + 2B\eta} - \frac{\eta_0}{1 + B\left(\eta_0 + \eta_1\right)}\right], \\
\frac{d\eta_0}{dz} &= C\eta_0\left[-\frac{\eta}{1 + 2B\eta} + \frac{\eta_1}{1 + B\left(\eta_0 + \eta_1\right)}\right].
\end{aligned} \tag{23}$$

To prove stability of the equilibrium point (η, η) we look for a Lyapunov function of the system (23) in the form

$$V_L(\eta_0, \eta_1) = \eta \ln\left(\frac{\eta}{\eta_0}\right) + \eta \ln\left(\frac{\eta}{\eta_1}\right) + \frac{1 + 2B\eta}{B} \ln\left[\frac{1 + B(\eta_0 + \eta_1)}{1 + 2B\eta}\right]. \tag{24}$$

Taking the derivative along trajectories of the system (23) we arrive at

$$\frac{dV_L}{dz} = -\frac{\eta}{\eta_0}\frac{d\eta_0}{dz} - \frac{\eta}{\eta_1}\frac{d\eta_1}{dz} + \frac{1 + 2B\eta}{1 + B(\eta_0 + \eta_1)}\frac{d}{dz}(\eta_0 + \eta_1). \tag{25}$$

Replacing $d\eta_0/dz$ and $d\eta_1/dz$ with the right hand sides of Eq. (23), we find

$$\frac{dV_L}{dz} = -C\eta\left[-\frac{\eta}{1+2B\eta} + \frac{\eta_1}{1+B\left(\eta_0+\eta_1\right)}\right] - C\eta\left[\frac{\eta}{1+2B\eta} - \frac{\eta_0}{1+B\left(\eta_0+\eta_1\right)}\right]$$
$$-\frac{C\eta(\eta_0-\eta_1)}{1+B\left(\eta_0+\eta_1\right)} = 0. \tag{26}$$

Hence, V_L is constant along trajectories of Eq. (23). In addition, it is straightforward to show that V_L attains its minimum at (η,η). Since $V_L(\eta,\eta) = 0$, it follows that $V_L(\eta_0,\eta_1) \geq 0$ for any (η_0,η_1) such that $\eta_0 > 0$ and $\eta_1 > 0$. Combining these results we conclude that V_L is a Lyapunov function for Eq. (23) and that the equilibrium state (η,η) is a center [48, 49]. Consequently, (η,η) is a stable equilibrium point and deviations of the initial amplitude values from η lead to oscillatory dynamics of $\eta_0(z)$ and $\eta_1(z)$. This means that the XPM perturbation does not change the stability properties of the equilibrium state.

To illustrate these conclusions we numerically solve Eq. (23) by use of a fourth-order Runge-Kutta scheme. For concreteness we consider a 2-channel transmission system operating at 160 Gbits/s per channel with time slot width $T = 5$. In this system the pulse width is 1.25 ps and $\epsilon_R = 0.0048$. Notice that WDM transmission at 160 Gbits/s per channel has received much attention in recent years both theoretically [51] and experimentally [52–54]. Taking $\beta_2 = -0.5\text{ps}^2\text{km}^{-1}$ and $\gamma = 4\text{W}^{-1}\text{km}^{-1}$ we obtain $P_0 = 80$ mW for the soliton peak power. The dimensionless final propagation distance is taken as $z_f = 1280$ corresponding to propagation over $X_f = 8000$ km, but the main dynamical features are observed already at much shorter distances. Without loss of generality we choose $\eta = 1$, so that the equilibrium state is $(1,1)$. Figure 6 shows the z-dependence of η_1 and η_0 with the initial condition $\eta_1(0) = 1.1$ and $\eta_0(0) = 0.9$ for $\Delta\beta = 2.0$ (a) and $\Delta\beta = 10.0$ (b). The latter values of $\Delta\beta$ correspond to interchannel frequency spacing of $\Delta\nu = 250$ GHz and $\Delta\nu = 1250$ GHz, respectively. In both cases the amplitudes exhibit oscillations about the equilibrium value in accordance with the prediction of the analytic calculations. Similar oscillatory dynamics is observed for other initial conditions and other values of $\Delta\beta$. Furthermore, as can be seen from Fig. 7, all solutions curves in the phase plane are closed. Thus, our numerical simulations validate the predictions about stability of the equilibrium state in the presence of XPM.

B. Effects of Raman self frequency shift

The Raman-induced SFS experienced by the jth-channel solitons is given by [55–57]

$$\frac{d\beta_j}{dz} = -\frac{8}{15}\epsilon_R \eta_j^4(z), \tag{27}$$

where we explicitly take into account the coupling of the frequency shift to the amplitude. Consider the effects of the Raman SFS on amplitude dynamics in a two-channel system consisting of channels 0 and 1. Since in general $\eta_0(z) \neq \eta_1(z)$, the Raman-induced SFS can lead to z-dependence of the frequency difference $\beta_{10}(z) = \beta_1(z) - \beta_0(z)$, which in turn would lead to z-dependence of the inter-collision distance $\Delta z_c^{(1)} = T/(2\beta_{10})$. Therefore, the impact of the Raman SFS on amplitude dynamics in a two-channel system can be taken into account by replacing the constant frequency difference $\Delta\beta$ by the z-dependent frequency difference $\beta_{10}(z)$ in the equations for η_0 and η_1, and by using relation (27) to obtain the dynamic equation for β_{10}. This calculation yields the following system:

$$\begin{aligned}
\frac{d\eta_1}{dz} &= \eta_1 \left(g_1 - \frac{C}{\Delta\beta}\beta_{10}\eta_0 \right), \\
\frac{d\eta_0}{dz} &= \eta_0 \left(g_0 + \frac{C}{\Delta\beta}\beta_{10}\eta_1 \right), \\
\frac{d\beta_{10}}{dz} &= -\frac{8}{15}\epsilon_R \left(\eta_1^4 - \eta_0^4 \right).
\end{aligned} \tag{28}$$

Looking for equilibrium states of the system (28) in the form $(\eta, \eta, \Delta\beta)$ we obtain $g_1 = -g_0 = C\eta$ for the gain/loss coefficients. Comparing this result with the result obtained in section II for the unperturbed model we see that the Raman-induced SFS does not change the values of the gain/loss coefficients that are required for maintaining an equilibrium state with equal amplitudes. Using the values $g_1 = -g_0 = C\eta$ we can rewrite the system (28) in a simpler form,

$$\begin{aligned}
\frac{d\eta_1}{dz} &= C\eta_1 \left(\eta - \beta_{10}\eta_0/\Delta\beta \right), \\
\frac{d\eta_0}{dz} &= C\eta_0 \left(-\eta + \beta_{10}\eta_1/\Delta\beta \right), \\
\frac{d\beta_{10}}{dz} &= -\frac{8}{15}\epsilon_R \left(\eta_1^4 - \eta_0^4 \right).
\end{aligned} \tag{29}$$

We study the stability of the equilibrium state $(\eta, \eta, \Delta\beta)$ of (29) by linear stability analysis and by numerical simulations. Linear stability analysis predicts a bifurcation at $\Delta\beta_{bif} =$

$(16T\eta^3/15)^{1/2}$. For $\Delta\beta > \Delta\beta_{bif}$ the Jacobian matrix of (29) has two purely imaginary eigenvalues and one zero eigenvalue, while for $\Delta\beta < \Delta\beta_{bif}$ all three eigenvalues are real. In the latter case one eigenvalue is positive, another is negative, and the third one is zero. For $\Delta\beta = \Delta\beta_{bif}$ all three eigenvalues are equal to zero. Based on this analysis one might suspect that the equilibrium state $(\eta, \eta, \Delta\beta)$ becomes unstable for $\Delta\beta < \Delta\beta_{bif}$. However, since $(\eta, \eta, \Delta\beta)$ remains a non-hyperbolic equilibrium point, linear stability calculations might fail [48, 49] and one has to resort to numerical simulations to study stability.

We perform numerical simulations with Eq. (29) for the same two-channel system that was considered in subsection III A. Choosing $\eta = 1$, the equilibrium state is $(1, 1, \Delta\beta)$ and the bifurcation value predicted by linear stability analysis is $\Delta\beta_{bif} \simeq 2.31$. Figure 8 shows the z-dependence of the amplitudes and frequency difference for $\Delta\beta = 2.0$ (a) and $\Delta\beta = 5.0$ (b). The initial conditions are $\eta_1(0) = 1.001$, $\eta_0(0) = 0.999$, and $\beta_{10}(0) = 1.999$ in (a), and $\eta_1(0) = 1.1$, $\eta_0(0) = 0.9$, and $\beta_{10}(0) = 5.1$ in (b). One observes that in (a) $\eta_1(z)$, $\eta_0(z)$, and $\beta_{10}(z)$ tend away from their equilibrium values $(1, 1, 2)$, while in (b) $\eta_1(z)$, $\eta_0(z)$, and $\beta_{10}(z)$ oscillate about their equilibrium values $(1, 1, 5)$. Similar dynamic behavior is obtained for other initial conditions in the neighborhood of $(1, 1, 2)$ or $(1, 1, 5)$. Based on these observations we conclude that the equilibrium state $(1, 1, 2)$ is unstable, whereas $(1, 1, 5)$ is stable, in agreement with linear stability analysis. This conclusion is further supported by the corresponding phase portraits that are shown in Fig. 9. For the system with $\Delta\beta = 2.0$ the trajectories starting in the vicinity of $(1, 1, 2)$ tend away from $(1, 1, 2)$. In contrast, for the system with $\Delta\beta = 5.0$ trajectories in the vicinity of $(1, 1, 5)$ are closed curves centered about $(1, 1, 5)$.

To further investigate the stability properties of a generic equilibrium point $(\eta, \eta, \Delta\beta)$ we perform detailed analysis of numerical simulations data for η and $\Delta\beta$ values close to the bifurcation line predicted by linear stability calculations: $\Delta\beta_{bif} \simeq 2.31\eta^{1.5}$. Figure 10 is the bifurcation diagram obtained by this analysis. It is seen that the bifurcation line obtained by numerical solution of Eq. (29) closely agrees with the line predicted by linear stability computations despite of the fact that $(\eta, \eta, \Delta\beta)$ is a non-hyperbolic equilibrium state. Notice that the points in the $\eta - \Delta\beta$ plane that are above the bifurcation line are stable, while those that are below the bifurcation line are unstable. Thus, transmission in the two-channel system described in subsection III A becomes unstable for frequency spacing values smaller than $2.31\eta^{1.5}$.

C. Effects of Raman cross frequency shift

The second effect of delayed Raman response on a single collision between a jth-channel soliton and a kth-channel soliton is an $O(\epsilon_R/|\beta_j - \beta_k|)$ frequency shift [7, 9–11, 15, 58]. This Raman-induced XFS is given by [15, 17, 18]

$$\Delta\beta_j = -\frac{8\epsilon_R \eta_j^2 \eta_k}{3|\beta_k - \beta_j|}. \tag{30}$$

We now consider the impact of this frequency shift on amplitude dynamics in a two-channel system. Since in general the amplitudes η_0 and η_1 vary with z, the frequency shifts might lead to z-dependence of the frequency difference β_{10}. In order to construct the perturbed model describing the effects of the Raman XFS we first obtain an equation for the dynamics of β_{10}. Using Eq. (30) we find $d\beta_0/dz = -16\epsilon_R\eta_0^2\eta_1/(3T)$ and $d\beta_1/dz = -16\epsilon_R\eta_0\eta_1^2/(3T)$. Combining these relations with the definition of β_{10} we arrive at

$$\frac{d\beta_{10}}{dz} = -16\epsilon_R\eta_0\eta_1\left(\eta_1 - \eta_0\right)/(3T). \tag{31}$$

In addition, we replace the constant frequency difference $\Delta\beta$ by the z-dependent frequency difference $\beta_{10}(z)$ in the equations for η_0 and η_1 to obtain

$$\begin{aligned}
\frac{d\eta_1}{dz} &= \eta_1\left(g_1 - \frac{C}{\Delta\beta}\beta_{10}\eta_0\right), \\
\frac{d\eta_0}{dz} &= \eta_0\left(g_0 + \frac{C}{\Delta\beta}\beta_{10}\eta_1\right).
\end{aligned} \tag{32}$$

Equations (31) and (32) represent the perturbed model for amplitude dynamics in the presence of the Raman XFS.

We look for equilibrium states of the model in the form $(\eta, \eta, \Delta\beta)$ and find $g_1 = -g_0 = C\eta$ for the gain/loss coefficients. Therefore, the Raman XFS does not modify the values of the gain/loss coefficients required for maintaining an equilibrium state with equal amplitudes. Substituting $g_1 = -g_0 = C\eta$ into Eq. (32) we obtain the following simpler form of the model:

$$\begin{aligned}
\frac{d\eta_1}{dz} &= C\eta_1\left(\eta - \beta_{10}\eta_0/\Delta\beta\right), \\
\frac{d\eta_0}{dz} &= C\eta_0\left(-\eta + \beta_{10}\eta_1/\Delta\beta\right), \\
\frac{d\beta_{10}}{dz} &= -16\epsilon_R\eta_0\eta_1\left(\eta_1 - \eta_0\right)/(3T).
\end{aligned} \tag{33}$$

It is possible to show that $V_X(\eta_1, \eta_0, \beta_{10}) = 8\eta_0\eta_1/3 + \beta_{10}^2$ is a conserved quantity for the system (33). However, this does not guarantee the stability of the equilibrium point. Linear stability analysis predicts bifurcation at $\Delta\beta_{bif} = (8/3)^{1/2}\eta$. For $\Delta\beta > \Delta\beta_{bif}$ the Jacobian matrix of (33) has two purely imaginary eigenvalues and one zero eigenvalue, while for $\Delta\beta < \Delta\beta_{bif}$ all three eigenvalues are real. In the latter case one eigenvalue is positive, another is negative, and the third one is zero. For $\Delta\beta = \Delta\beta_{bif}$ all three eigenvalues are equal to zero. Based on this analysis one suspects that the equilibrium state $(\eta, \eta, \Delta\beta)$ becomes unstable for $\Delta\beta < \Delta\beta_{bif}$.

Since $(\eta, \eta, \Delta\beta)$ is a non-hyperbolic equilibrium point linear stability calculations might lead to erroneous conclusions [48, 49]. We therefore investigate the stability of $(\eta, \eta, \Delta\beta)$ by numerical simulations with Eq. (33). For concreteness we consider the two-channel system described in subsection III A. Choosing $\eta = 1$, the equilibrium state is $(1, 1, \Delta\beta)$ and the bifurcation value predicted by linear stability analysis is $\Delta\beta_{bif} \simeq 1.63$. Figure 11 shows the dynamics of the amplitudes and frequency difference for $\Delta\beta = 1.5$ (a) and $\Delta\beta = 5.0$ (b). The initial conditions are $\eta_1(0) = 1.001$, $\eta_0(0) = 0.999$, and $\beta_{10}(0) = 1.499$ in (a), and $\eta_1(0) = 1.2$, $\eta_0(0) = 0.9$, and $\beta_{10}(0) = 5.05$ in (b). It is observed that in (a) $\eta_1(z)$, $\eta_0(z)$, and $\beta_{10}(z)$ tend away from their equilibrium values $(1, 1, 1.5)$, while in (b) $\eta_1(z)$, $\eta_0(z)$, and $\beta_{10}(z)$ oscillate about the equilibrium values $(1, 1, 5)$. Additional numerical simulations with other initial conditions in the vicinity of $(1, 1, 1.5)$ or $(1, 1, 5)$ show the same dynamical behavior. We therefore conclude that the equilibrium state $(1, 1, 1.5)$ is unstable, while $(1, 1, 5)$ is stable, in agreement with linear stability analysis. This conclusion is also supported by the corresponding phase portraits.

To check the stability of a generic equilibrium state $(\eta, \eta, \Delta\beta)$ we carefully analyze results of numerical simulations with Eq. (33) for different η and $\Delta\beta$ values. We pay special attention to the region in the η-$\Delta\beta$ plane that is in the close neighborhood of the bifurcation line $\Delta\beta_{bif} \simeq 1.63\eta$, predicted by linear stability computations. Figure 12 shows the bifurcation diagram that is obtained by our analysis. It is seen that the bifurcation line obtained by numerical simulations is in good agreement with the line predicted by linear stability calculations, despite of the non-hyperbolic character of $(\eta, \eta, \Delta\beta)$. Notice that equilibrium points lying below the line $\Delta\beta = 1.63\eta$ are unstable, while those lying above it are stable. As a practical consequence we note that transmission in the two-channel system described in subsection III A is unstable for frequency spacing values smaller than 1.63η.

IV. CONCLUSIONS

We studied the deterministic effects of inter-pulse Raman crosstalk in amplified WDM optical fiber transmission systems. We considered conventional optical solitons as an example for the pulses carrying the information and assumed that the pulse sequences in all frequency channels are deterministic and that the sequences are either infinitely long or are subject to periodic temporal boundary conditions. The first setup approximates return-to-zero (RZ) differential-phase-shift-keyed (DPSK) long-haul transmission, while the second one corresponds to RZ DPSK closed fiber loop experiments. We assumed in addition that the constant gain/loss in each frequency channel is determined by the difference between distributed amplifier gain and fiber loss. Under these assumptions we showed that the dynamics of pulse amplitudes in an N-channel transmission line is described by a system of N coupled nonlinear ordinary differential equations (ODEs), having the form of an N-dimensional predator-prey model. We calculated the gain/loss coefficients required for maintaining an equilibrium state with equal non-zero amplitudes in all channels, and showed that high-frequency channels should be overamplified, while low-frequency channels should be underamplified compared with the middle (reference) channel. This means that the net gain/loss profile should *not* be flat with respect to the frequency. With these values of the gain/loss coefficients we proved stability of equilibrium states with non-zero amplitudes in all channels by constructing Lyapunov functions for the system of ODEs. The stability was found to be independent of the exact details of the approximation for the Raman gain curve. Furthermore, since the Lyapunov functions are conserved quantities for the system, typical dynamics of the amplitudes for initial conditions that are off the equilibrium points is oscillatory.

In an actual optical fiber line Raman crosstalk is not the only process impacting pulse dynamics. It is therefore important to understand the manner in which other physical processes perturb the Raman-induced amplitude dynamics described above. In this study we concentrated on the effects of three perturbations due to cross phase modulation (XPM), Raman self frequency shift (SFS) and Raman cross frequency shift (XFS). For each of these physical processes we constructed the corresponding perturbed model for an N-channel system and studied the dynamics in a two-channel system. For XPM-perturbed two-channel transmission we found that the gain/loss coefficients required for maintaining an equilib-

rium state with equal non-zero amplitudes are smaller compared with the values in the unperturbed case. This is explained by noting that the XPM-induced position shifts tend to increase the inter-collision distance and thus to decrease the rate of collisions. In contrast, the stability of the equilibrium state with equal non-zero amplitudes is not changed by XPM, i.e., the equilibrium state remains a center. For two-channel systems perturbed by Raman SFS or Raman XFS we found that the values of the gain/loss coefficients required for maintaining the equilibrium state are the same as in the unperturbed case. However, the stability properties of the equilibrium state change as the frequency difference between the channels is decreased or increased, i.e., the system undergoes a bifurcation. The bifurcation curves are given by $\Delta\beta_{bif} = (16T\eta^3/15)^{1/2}$ for the perturbed model with Raman SFS and $\Delta\beta_{bif} = (8/3)^{1/2}\eta$ for the perturbed model with Raman XFS. In both models, for a fixed value of η, two-channel transmission with $\Delta\beta > \Delta\beta_{bif}$ is stable, while two-channel transmission with $\Delta\beta < \Delta\beta_{bif}$ is unstable. We therefore conclude that the Raman-induced interplay between amplitude dynamics and frequency dynamics sets a bound on the smallest frequency spacing for stable transmission.

In summary, our study provides a quantitative explanation to the stability of WDM DPSK transmission against Raman crosstalk effects. This stability was demonstrated in experiments in a closed fiber loop [28]. The stable behavior of Raman-induced amplitude dynamics in DPSK transmission is very different from the intermittent dynamic behavior exhibited by pulse parameters in on-off-keyed (OOK) transmission due to the interplay between Raman crosstalk and bit-pattern randomness [4, 6, 17–19]. This different dynamic behavior is an important advantage of DPSK transmission over OOK transmission.

Appendix A: Perturbed models in WDM transmission with $2N + 1$ channels

In this appendix we derive the perturbed models for Raman-induced amplitude dynamics in the presence of XPM and Raman SFS and XFS for WDM transmission lines with $2N + 1$ channels.

1. Cross phase modulation

The rate of collisions of a soliton from the jth channel with solitons from the the kth channel in the *unperturbed* model is

$$R^u_{jk} = |k-j|/\Delta z^{(1)}_c, \tag{A1}$$

where $\Delta z^{(1)}_c = T/(2\Delta\beta)$ is constant. Thus, Eq. (4) for the change of the soliton amplitude in the interval $(z_{l-1}, z_{l-1}+\Delta z^{(1)}_c]$ in the *unperturbed* model can be written as

$$\begin{aligned}\eta_j(z_{l-1}+\Delta z^{(1)}_c) &= \eta_j(z_{l-1}) + g_j\eta_j(z_{l-1})\Delta z^{(1)}_c \\ &+2\epsilon_R\Delta z^{(1)}_c\sum_{k=-N}^{N} R^u_{jk}\mathrm{sgn}(k-j)f(|j-k|)\eta_j(z_{l-1})\eta_k(z_{l-1}).\end{aligned} \tag{A2}$$

In the *perturbed* transmission system, Eq. (A1) is replaced by

$$R^p_{jk}(z) = |k-j|/\Delta z^{(1)}_{cjk}(z), \tag{A3}$$

where the z-dependent inter-collision distance $\Delta z^{(1)}_{cjk}$ is affected by the XPM-induced position shifts. Replacing R^u_{jk} by R^p_{jk} in Eq. (A2) while employing relation (A3) we arrive at

$$\begin{aligned}\eta_j(z_{l-1}+\Delta z^{(1)}_c) &= \eta_j(z_{l-1}) + g_j\eta_j(z_{l-1})\Delta z^{(1)}_c \\ &+2\epsilon_R\Delta z^{(1)}_c\sum_{k=-N}^{N} \frac{k-j}{\Delta z^{(1)}_{cjk}(z_{l-1})}f(|j-k|)\eta_j(z_{l-1})\eta_k(z_{l-1}).\end{aligned} \tag{A4}$$

In order to find an expression for $\Delta z^{(1)}_{cjk}(z)$ we write down an equation for the location of the collision of the soliton from the zeroth time slot in the jth channel with the soliton from the $l(j-k)$ time slot in the kth channel: $y_{k,l(j-k)}(z_l) = y_{j,0}(z_l)$. Taking into account the different group velocities and summing over all XPM-induced position shifts during the collisions we arrive at the following generalization of Eq. (19):

$$\begin{aligned}&y_{k,l(j-k)}(z_{l-1}) + 2k\Delta\beta\Delta z^{(1)}_{cjk}(z_{l-1}) + \frac{4}{(\Delta\beta)^2}\sum_{m=-N}^{N}\eta_m(z_{l-1})\frac{|m-k|\mathrm{sgn}(\beta_m-\beta_k)(1-\delta_{mk})}{(m-k)^2} \\ &= y_{j,0}(z_{l-1}) + 2j\Delta\beta\Delta z^{(1)}_{cjk}(z_{l-1}) + \frac{4}{(\Delta\beta)^2}\sum_{m=-N}^{N}\eta_m(z_{l-1})\frac{|m-j|\mathrm{sgn}(\beta_m-\beta_j)(1-\delta_{mj})}{(m-j)^2},\end{aligned} \tag{A5}$$

where δ_{ij} is the Kronecker delta function. Solution of Eq. (A5) for $\Delta z^{(1)}_{cjk}(z_{l-1})$ yields

$$\Delta z^{(1)}_{cjk}(z_{l-1}) = \frac{T}{2\Delta\beta}\left\{1 + \frac{4}{T(j-k)(\Delta\beta)^2}\sum_{m=-N}^{N}\eta_m(z_{l-1})\left[\frac{1-\delta_{mk}}{m-k} - \frac{1-\delta_{mj}}{m-j}\right]\right\}. \tag{A6}$$

Taking the continuum limit in Eqs. (A4) and (A6) we obtain

$$\frac{d\eta_j}{dz} = \eta_j \left[g_j + 2\epsilon_R \sum_{k=-N}^{N} \frac{k-j}{\Delta z_{cjk}^{(1)}} f(|j-k|)\eta_k \right]. \tag{A7}$$

Equation (A7) together with Eq. (A6) (with z_{l-1} replaced by z) represent the perturbed model for Raman-induced amplitude dynamics in the presence of XPM in WDM transmission systems with $2N+1$ channels.

2. Raman self and cross frequency shifts

Consider the perturbed model with the Raman-induced SFS. The change in the amplitude of a jth-channel soliton within the interval $(z_{l-1}, z_{l-1} + \Delta z_c^{(1)}]$ is still given by Eq. (A4). However, now the z-dependent inter-collision distance $\Delta z_{cjk}^{(1)}$ is given by

$$\Delta z_{cjk}^{(1)}(z_{l-1}) = (k-j)T/(2\beta_{kj}(z_{l-1})), \tag{A8}$$

where $\beta_{kj}(z) = \beta_k(z) - \beta_j(z)$. The dynamics of β_{kj} is governed by

$$\frac{d\beta_{kj}}{dz} = -\frac{8}{15}\epsilon_R \left(\eta_k^4 - \eta_j^4\right). \tag{A9}$$

Substituting relation (A8) into Eq. (A4) and going to the continuum limit we obtain

$$\frac{d\eta_j}{dz} = \eta_j \left[g_j + \frac{4\epsilon_R}{T} \sum_{k=-N}^{N} f(|j-k|)\beta_{kj}\eta_k \right]. \tag{A10}$$

Equations (A9) and (A10) with $-N \le j,k \le N$ describe the Raman-induced amplitude dynamics in the presence of Raman SFS in transmission systems with $2N+1$ channels. It is straightforward to show that the gain/loss coefficients g_j that are required for maintaining an equilibrium state with equal non-zero amplitudes in all channels are given by Eq. (6), that is, the values of these coefficients are not modified by the Raman SFS.

Turning to the perturbed model with Raman XFS we observe that amplitude dynamics is described by Eq. (A10). To obtain the dynamic equation for the frequency difference β_{kj} we first compute the change in the frequency experienced by a soliton in the jth channel within the interval $(z_{l-1}, z_{l-1} + \Delta z_c^{(1)}]$. Employing Eq. (30) and summing over all collisions we arrive at

$$\beta_j(z_{l-1} + \Delta z_c^{(1)}) = \beta_j(z_{l-1}) - \frac{8\epsilon_R}{3\Delta\beta}\eta_j^2(z_{l-1}) \sum_{k=-N}^{N} \eta_k(z_{l-1})(1-\delta_{kj}). \tag{A11}$$

The continuum limit of Eq. (A11) is

$$\frac{d\beta_j}{dz} = -\frac{16\epsilon_R}{3T}\eta_j^2 \sum_{k=-N}^{N} \eta_k(1-\delta_{kj}), \tag{A12}$$

and therefore the dynamics of $\beta_{kj}(z)$ is governed by

$$\frac{d\beta_{kj}}{dz} = -\frac{16\epsilon_R}{3T}\left[\eta_k\eta_j(\eta_k-\eta_j) + \sum_{m=-N}^{N} \eta_m(\eta_k^2-\eta_j^2)(1-\delta_{mk})(1-\delta_{mj})\right]. \tag{A13}$$

Thus, the perturbed model for Raman-induced amplitude dynamics in the presence of Raman XFS is given by Eqs. (A10) and (A13), where $-N \le j,k \le N$. A simple calculation shows that the values of the gain/loss coefficients required to maintain an equilibrium state with equal non-zero amplitudes in all frequency channels are the same as in the unperturbed model.

---

[1] G. P. Agrawal, *Nonlinear Fiber Optics* (Academic, San Diego, CA, 2001).

[2] R. H. Stolen, Proc. IEEE **68**, 1232 (1980).

[3] A. R. Chraplyvy, Electron. Lett. **20**, 58 (1984).

[4] F. Forghieri, R. W. Tkach, and A. R. Chraplyvy, IEEE Photon. Technol. Lett. **7**, 101 (1995).

[5] D. N. Christodoulides and R. B. Jander, IEEE Photon. Technol. Lett. **8**, 1722 (1996).

[6] K.-P. Ho, J. Lightwave Technol. **18**, 915 (2000).

[7] S. Chi and S. Wen, Opt. Lett. **14**, 1216 (1989).

[8] B. A. Malomed, Phys. Rev. A **44**, 1412 (1991).

[9] S. Kumar, Opt. Lett. **23**, 1450 (1998).

[10] A. Peleg, Opt. Lett. **29**, 1980 (2004).

[11] T. I. Lakoba and D. J. Kaup, Opt. Lett. **24**, 808 (1999).

[12] D. Cotter and A. M. Hill, Electron. Lett. **20**, 185 (1984).

[13] A. R. Sarkar, M. N. Islam and M.G. Mostafa, Opt. Quantum Electron. **39**, 659 (2007).

[14] M. Muktoyuk and S. Kumar, IEEE Photon. Technol. Lett. **15**, 1222 (2003).

[15] Y. Chung and A. Peleg, Nonlinearity **18**, 1555 (2005).

[16] T. Yamamoto and S. Norimatsu, J. Lightwave Technol. **21**, 2229 (2003).

[17] A. Peleg, Phys. Lett. A **360**, 533 (2007).

[18] Y. Chung and A. Peleg, Phys. Rev. A **77**, 063835 (2008).

[19] A. Peleg, Phys. Lett. A **373**, 2734 (2009).

[20] X. Zhou and M. Birk, J. Lightwave Technol. **24**, 1218 (2006).

[21] D. Mazroa, S. Zsigmond, and T. Cinkler, Photon. Network Commun. **18**, 77 (2009).

[22] B. Colella, F. Effenberger, C. Shimer, and F. Tian, "Raman Crosstalk Control in Passive Optical Networks", in *Proc. Fiber Opt. Eng. Conf.*, Anaheim, CA, 2006, paper NWD6.

[23] H. Kim, S. B. Jun, and Y. C. Chung, IEEE Photon. Technol. Lett. **19**, 695 (2007).

[24] Z. A. T. Al-Qazwini, M. K. Abdullah, and M. B. Mokhtar, Opt. Eng. **48**, 015001 (2009).

[25] F. Vanholsbeeck, S. Coen, P. Emplit, M. Haelterman and T. Sylvestre, Opt. Commun. **250**, 191 (2005).

[26] C. Xu, X. Liu, and X. Wei, IEEE J. Quantum Electron. **10**, 281 (2004).

[27] A. H. Gnauck and P. J. Winzer, J. Lightwave Technol. **23**, 115 (2005).

[28] V. J. Mazurczyk, G. Shaulov, and E. A. Golovchenko, IEEE Photon. Technol. Lett. **12**, 1573 (2000).

[29] H. Kim, J. H. Lee, and H. Ji, Opt. Express **16**, 20687 (2008).

[30] V. E. Zakharov and A. B. Shabat, Sov. Phys. JETP **34**, 62 (1972).

[31] M. N. Islam, ed., *Raman Amplifiers for Telecommunications 1: Physical Principles* (Springer, New York, 2004).

[32] C. Headley and G. P. Agrawal, eds., *Raman Amplification in Fiber Optical Communication Systems* (Elsevier, San Diego, CA, 2005).

[33] L. F. Mollenauer, A. Grant, X. Liu, X. Wei, C. Xie, and I. Kang, Opt. Lett. **28**, 2043 (2003).

[34] D. F. Grosz, A. Agarwal, S. Banerjee, D. N. Maywar, A. P. Küng, J. Lightwave Technol. **22**, 423 (2004).

[35] C. Rasmussen, T. Fjelde, J. Bennike, F. Liu, S. Dey, B. Mikkelsen, P. Mamyshev, P. Serbe, P. van der Wagt, Y. Akasaka, D. Harris, D. Gapontsev, V. Ivshin, and P. Reeves-Hall, J. Lightwave Technol. **22**, 203 (2004).

[36] Z. B. Xu, K. Rottwitt, C. Peucheret, and P. Jeppesen, IEEE Photon. Technol. Lett. **16**, 329 (2004).

[37] J. D. Ania-Castañón, T. J. Ellingham, R. Ibbotson, X. Chen, L. Zhang, and S. K. Turitsyn, Phys. Rev. Lett. **96**, 023902 (2006).

[38] L. F. Mollenauer and P. V. Mamyshev, IEEE J. Quantum Electron. **34**, 2089 (1998).

[39] A. H. Gnauck, R. W. Tkach, A. R. Chraplyvy, and T. Li, J. Lightwave Technol. **26**, 1032 (2008).

[40] V. Volterra, "Variations and fluctuations of the number of individuals in animal species living together", translated in *Animal Ecology*, R. N. Chapman, ed., (McGraw-Hill, 1931, New York).

[41] R. H. Stolen, J. P. Gordon, W. J. Tomlinson, and H. A. Haus, J. Opt. Soc. Am. B **6**, 1159 (1989).

[42] The dimensionless z in Eq. (1) is $z = (|\beta_2|X)/(2\tau_0^2)$, where X is the actual position, τ_0 is the soliton width, and β_2 is the second order dispersion coefficient. The dimensionless retarded time is $t = \tau/\tau_0$, where τ is the retarded time. The spectral width is $\nu_0 = 1/(\pi^2\tau_0)$ and the frequency difference is $\Delta\nu = (\pi\Delta\beta\nu_0)/2$. $\psi = E/\sqrt{P_0}$, where E is proportional to the electric field and P_0 is the peak power. The dimensionless second order dispersion coefficient is $d = -1 = \beta_2/(\gamma P_0\tau_0^2)$, where γ is the Kerr nonlinearity coefficient. The coefficient ϵ_R is given by $\epsilon_R = 0.006/\tau_0$, where τ_0 is in picoseconds.

[43] B. A. Malomed, Phys. Rev. A **43**, 3114 (1991).

[44] A. Peleg, M. Chertkov, and I. Gabitov, Phys. Rev. E **68**, 026605 (2003).

[45] A. Peleg, M. Chertkov, and I. Gabitov, J. Opt. Soc. Am. B **21**, 18 (2004).

[46] It is possible to show that the same model describes the drift part of the amplitude dynamics in RZ OOK transmission systems. See Refs. [17, 18] for a detailed derivation. Note that in this case the coefficient C in Eq. (5) is given by $C = 4\epsilon_R s\Delta\beta/T$, where s is the average fraction of occupied time slots.

[47] For transmission with an even number of channels Eq. (8) does not necessarily possess solutions other than the trivial solution. However, when the Raman gain is described by the triangular approximation Eq. (8) has infinitely many solutions even for a $2N$-channel system. These solutions are given by expressions similar to the ones in Eq. (9). The proof of stability of the corresponding equilibrium states is similar to the proof for transmission with an odd number of channels.

[48] M. W. Hirsch and S. Smale, *Differential Equations, Dynamical Systems, and Linear Algebra* (Academic Press, New York, 1974).

[49] S. Wiggins, *Introduction to Applied Nonlinear Dynamical Systems and Chaos* (Springer, New York, 2003).

[50] It is possible to show that Z_p is inversely proportional to ϵ_R.

[51] B. Cuenot, IEEE Photon. Technol. Lett. **15**, 864 (2003).

[52] A. H. Gnauck, G. Raybon, P. G. Bernasconi, J. Leuthold, C. R. Doerr, and L. W. Stulz, IEEE Photon. Technol. Lett. **15**, 1618 (2003).

[53] M. Daikoku, T. Miyazaki, I. Morita, H. Tanaka, F. Kubota, and M. Suzuki, IEEE Photon. Technol. Lett. **18**, 391 (2006).

[54] A. F. Abas, A. Hidayat, D. Sandel, B. Milivojevic, and R. Noe, Opt. Fiber Technol. **13**, 46 (2007).

[55] F. M. Mitschke and L. F. Mollenauer, Opt. Lett. **11**, 659 (1986).

[56] J. P. Gordon, Opt. Lett. **11**, 662 (1986).

[57] Y. Kodama and A. Hasegawa, IEEE J. Quantum Electron. **23**, 510 (1987).

[58] C. Headley III and G. P. Agrawal, J. Opt. Soc. Am. B **13**, 2170 (1996).

List of Figure Captions

Fig. 1. Amplitude dynamics for the two-channel system described by Eq. (13). (a) The z-dependence of η_{50} (solid curve) and η_0 (dotted curve) with the initial condition $\eta_{50}(0) = 1.2$ and $\eta_0(0) = 0.9$. (b) The corresponding phase portrait.

Fig. 2. Amplitude dynamics for the three-channel system described by Eq. (15). (a) The phase portrait. (1,1,1) is the second equilibrium point from the right. (b) The z-dependence of η_{50} (solid curve), η_0 (dotted curve), and η_{-50} (dashed curve), with the initial condition $\eta_{50}(0) = 0.8$, $\eta_0(0) = 0.9$, $\eta_{-50}(0) = 1.1$.

Fig. 3. The z-dependence of pulse amplitudes for the four-channel system described by Eq. (16) for $p = 0$ (a), and $p = 0.1$ (b). The initial condition is $\eta_{48}(0) = 1.2$, $\eta_{16}(0) = 1.1$, $\eta_{-16}(0) = 0.95$, and $\eta_{-48}(0) = 0.9$. The solid, dashed, dashed-dotted, and dotted curves represent $\eta_{48}(z)$, $\eta_{16}(z)$, $\eta_{-16}(z)$, and $\eta_{-48}(z)$, respectively.

Fig. 4. The z-dependence of the amplitudes of pulses in the $j = 48$ channel for $p = 0$ (a), and $p = 0.1$ (b). The initial condition is the same as in Fig 3 and the final propagation distance is $z_f = 2000$.

Fig. 5. The z-dependence of pulse amplitudes for a seven-channel system operating at 10 Gbits/s per channel. The initial amplitudes are $\eta_{180}(0) = 1.2$, $\eta_{120}(0) = 1.05$, $\eta_{60}(0) = 1.1$ $\eta_0(0) = 1.15$, $\eta_{-60}(0) = 0.98$, $\eta_{-120}(0) = 1.1$, and $\eta_{-180}(0) = 0.95$. The solid, dashed, dotted, and dashed-dotted curves in (a) represent $\eta_{180}(z)$, $\eta_{60}(z)$, $\eta_{-60}(z)$, and $\eta_{-180}(z)$, respectively. The solid, dashed, and dotted curves in (b) correspond to $\eta_{120}(z)$, $\eta_0(z)$, and $\eta_{-120}(z)$.

Fig. 6. The z-dependence of pulse amplitudes for the XPM-perturbed two-channel system described by Eq. (23) with $\Delta\beta = 2.0$ (a) and $\Delta\beta = 10.0$ (b). The initial condition is $\eta_1(0) = 1.1$ and $\eta_0(0) = 0.9$. The solid and dotted lines represent $\eta_1(z)$, and $\eta_0(z)$, respectively.

Fig. 7. The phase portrait for the XPM-perturbed two-channel system described by Eq. (23) with $\Delta\beta = 2.0$ (a) and $\Delta\beta = 10.0$ (b).

Fig. 8. The z-dependence of soliton amplitudes and frequency difference for a two-channel system perturbed by the Raman SFS [Eq. (29)]. (a) The dynamics with $\Delta\beta = 2.0$ and initial condition $\eta_1(0) = 1.001$, $\eta_0(0) = 0.999$, and $\beta_{10}(0) = 1.999$. (b) The dynamics with $\Delta\beta = 5.0$ and initial condition $\eta_1(0) = 1.1$, $\eta_0(0) = 0.9$, $\beta_{10}(0) = 5.1$. The solid, dashed and dotted lines represent $\eta_1(z)$, $\eta_0(z)$, and $\beta_{10}(z)$, respectively.

Fig. 9. The phase portraits for the two-channel system perturbed by the Raman SFS with $\Delta\beta = 2.0$ (a) and $\Delta\beta = 5.0$ (b).

Fig. 10. The bifurcation diagram for the two-channel system perturbed by the Raman SFS. The squares correspond to the bifurcation values obtained by numerical solution of Eq. (29), while the solid line is a fit of the form $\Delta\beta_{bif} = 2.30\eta^{1.51}$ for the numerical data. The dotted line represents the prediction of linear stability analysis: $\Delta\beta_{bif} \simeq 2.31\eta^{1.5}$.

Fig. 11. The z-dependence of soliton amplitudes and frequency difference for a two-channel system perturbed by the Raman XFS [Eq. (33)]. (a) The dynamics with $\Delta\beta = 1.5$ and initial condition $\eta_1(0) = 1.001$, $\eta_0(0) = 0.999$, and $\beta_{10}(0) = 1.499$. (b) The dynamics with $\Delta\beta = 5.0$ and initial condition $\eta_1(0) = 1.2$, $\eta_0(0) = 0.9$, $\beta_{10}(0) = 5.05$. The solid, dashed and dotted lines represent $\eta_1(z)$, $\eta_0(z)$, and $\beta_{10}(z)$, respectively.

Fig. 12. The bifurcation diagram for the two-channel system perturbed by the Raman XFS. The squares correspond to the bifurcation values obtained by numerical solution of Eq. (33), while the solid line is a fit of the form $\Delta\beta_{bif} = 0.04 + 1.64\eta$ for the numerical data. The dotted line is the prediction of linear stability analysis: $\Delta\beta_{bif} \simeq 1.63\eta$.

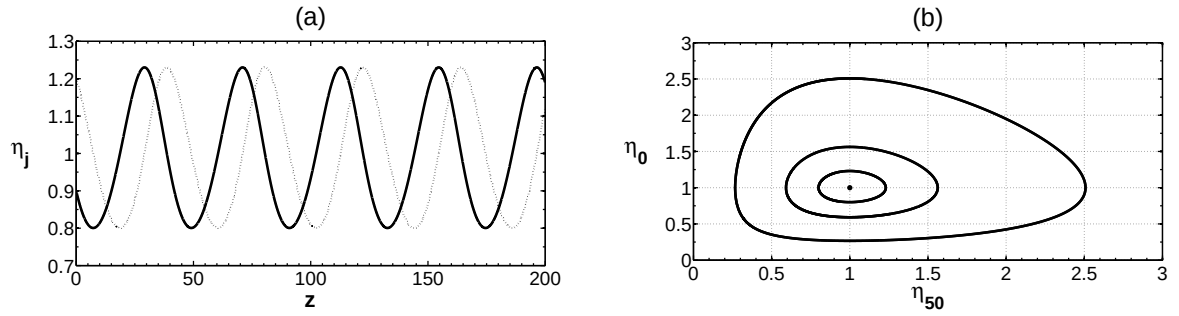

FIG. 1: Amplitude dynamics for the two-channel system described by Eq. (13). (a) The z-dependence of η_{50} (solid curve) and η_0 (dotted curve) with the initial condition $\eta_{50}(0) = 1.2$ and $\eta_0(0) = 0.9$. (b) The corresponding phase portrait.

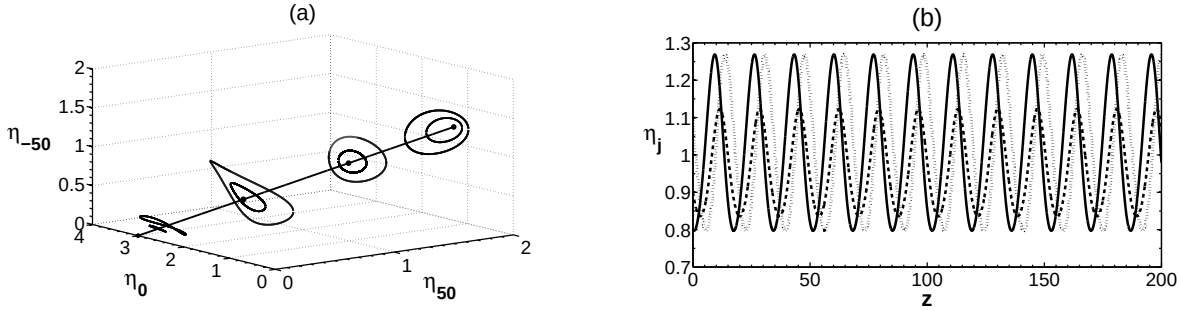

FIG. 2: Amplitude dynamics for the three-channel system described by Eq. (15). (a) The phase portrait. (1,1,1) is the second equilibrium point from the right. (b) The z-dependence of η_{50} (solid curve), η_0 (dotted curve), and η_{-50} (dashed curve), with the initial condition $\eta_{50}(0) = 0.8$, $\eta_0(0) = 0.9$, $\eta_{-50}(0) = 1.1$.

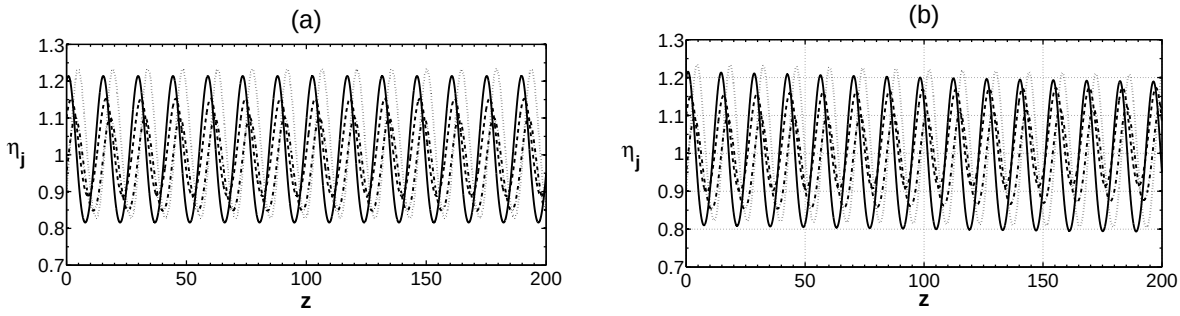

FIG. 3: The z-dependence of pulse amplitudes for the four-channel system described by Eq. (16) for $p = 0$ (a), and $p = 0.1$ (b). The initial condition is $\eta_{48}(0) = 1.2$, $\eta_{16}(0) = 1.1$, $\eta_{-16}(0) = 0.95$, and $\eta_{-48}(0) = 0.9$. The solid, dashed, dashed-dotted, and dotted curves represent $\eta_{48}(z)$, $\eta_{16}(z)$, $\eta_{-16}(z)$, and $\eta_{-48}(z)$, respectively.

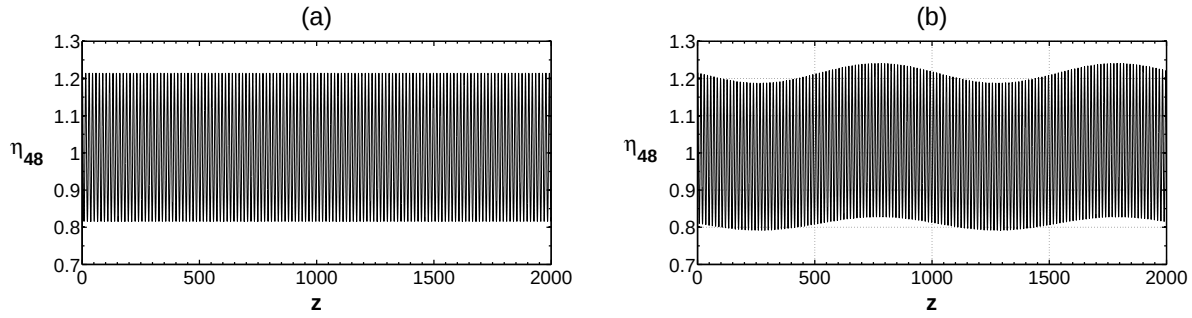

FIG. 4: The z-dependence of the amplitudes of pulses in the $j = 48$ channel for $p = 0$ (a), and $p = 0.1$ (b). The initial condition is the same as in Fig 3 and the final propagation distance is $z_f = 2000$.

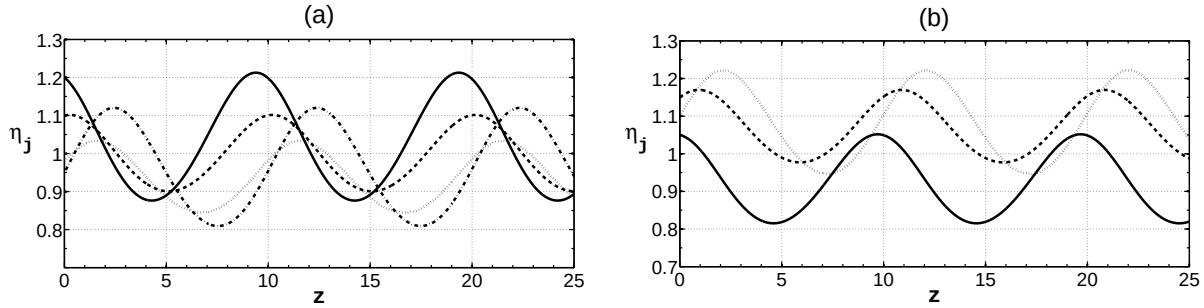

FIG. 5: The z-dependence of pulse amplitudes for a seven-channel system operating at 10 Gbits/s per channel. The initial amplitudes are $\eta_{180}(0) = 1.2$, $\eta_{120}(0) = 1.05$, $\eta_{60}(0) = 1.1$ $\eta_0(0) = 1.15$, $\eta_{-60}(0) = 0.98$, $\eta_{-120}(0) = 1.1$, and $\eta_{-180}(0) = 0.95$. The solid, dashed, dotted, and dashed-dotted curves in (a) represent $\eta_{180}(z)$, $\eta_{60}(z)$, $\eta_{-60}(z)$, and $\eta_{-180}(z)$, respectively. The solid, dashed, and dotted curves in (b) correspond to $\eta_{120}(z)$, $\eta_0(z)$, and $\eta_{-120}(z)$.

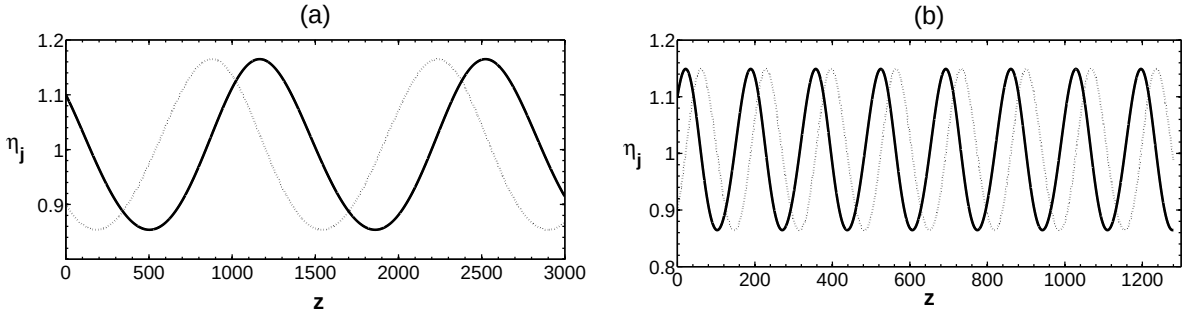

FIG. 6: The z-dependence of pulse amplitudes for the XPM-perturbed two-channel system described by Eq. (23) with $\Delta\beta = 2.0$ (a) and $\Delta\beta = 10.0$ (b). The initial condition is $\eta_1(0) = 1.1$ and $\eta_0(0) = 0.9$. The solid and dotted lines represent $\eta_1(z)$, and $\eta_0(z)$, respectively.

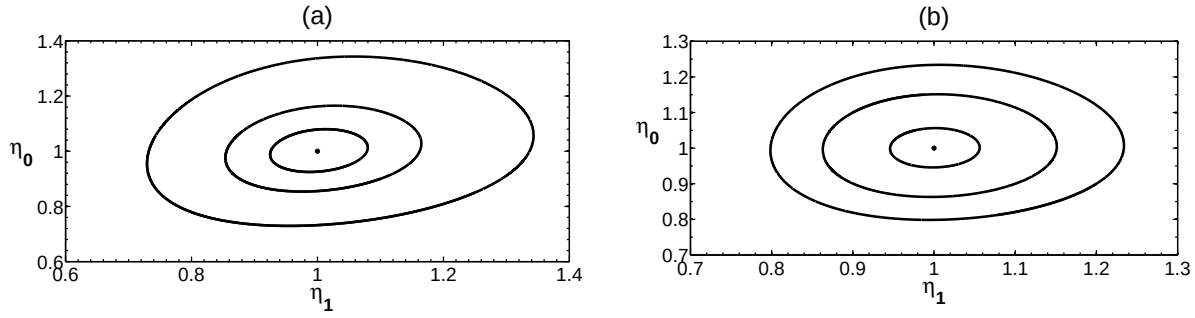

FIG. 7: The phase portrait for the XPM-perturbed two-channel system described by Eq. (23) with $\Delta\beta = 2.0$ (a) and $\Delta\beta = 10.0$ (b).

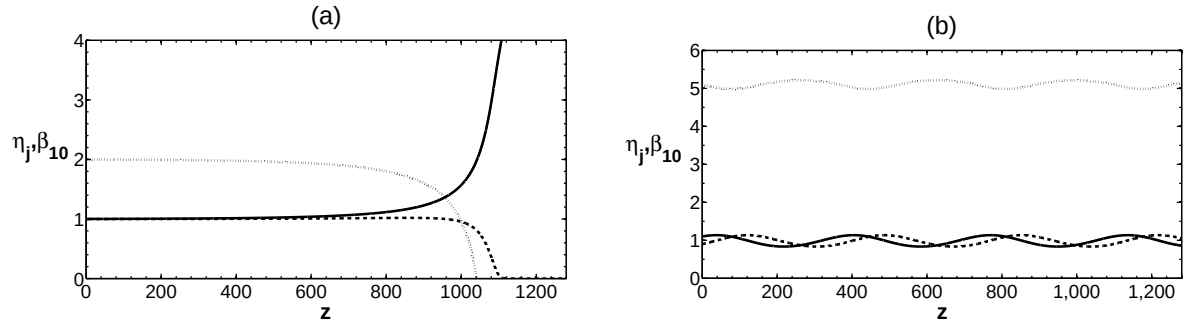

FIG. 8: The z-dependence of soliton amplitudes and frequency difference for a two-channel system perturbed by the Raman SFS [Eq. (29)]. (a) The dynamics with $\Delta\beta = 2.0$ and initial condition $\eta_1(0) = 1.001$, $\eta_0(0) = 0.999$, and $\beta_{10}(0) = 1.999$. (b) The dynamics with $\Delta\beta = 5.0$ and initial condition $\eta_1(0) = 1.1$, $\eta_0(0) = 0.9$, $\beta_{10}(0) = 5.1$. The solid, dashed and dotted lines represent $\eta_1(z)$, $\eta_0(z)$, and $\beta_{10}(z)$, respectively.

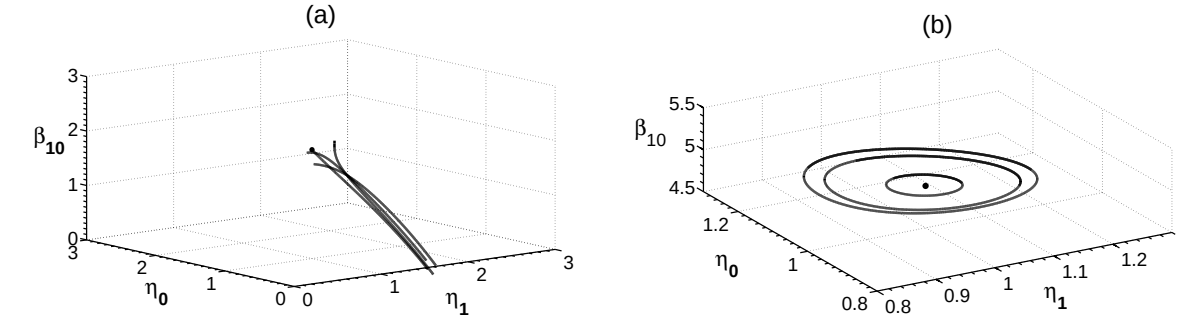

FIG. 9: The phase portraits for the two-channel system perturbed by the Raman SFS with $\Delta\beta = 2.0$ (a) and $\Delta\beta = 5.0$ (b).

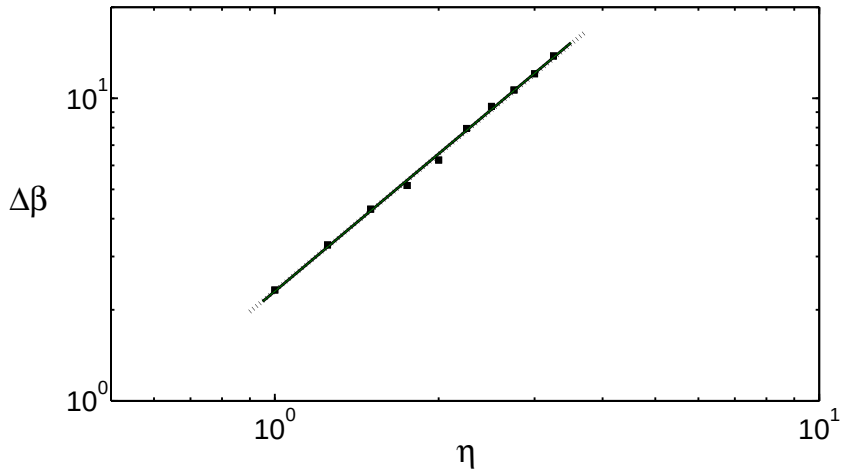

FIG. 10: The bifurcation diagram for the two-channel system perturbed by the Raman SFS. The squares correspond to the bifurcation values obtained by numerical solution of Eq. (29), while the solid line is a fit of the form $\Delta\beta_{bif} = 2.30\eta^{1.51}$ for the numerical data. The dotted line represents the prediction of linear stability analysis: $\Delta\beta_{bif} \simeq 2.31\eta^{1.5}$.

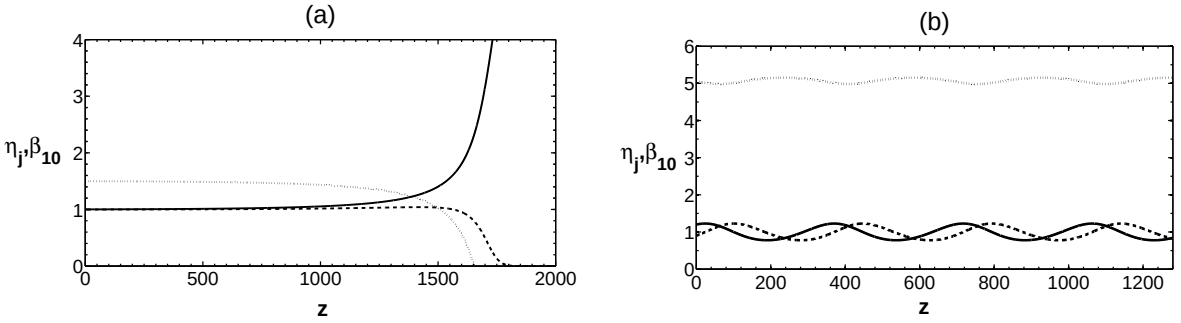

FIG. 11: The z-dependence of soliton amplitudes and frequency difference for a two-channel system perturbed by the Raman XFS [Eq. (33)]. (a) The dynamics with $\Delta\beta = 1.5$ and initial condition $\eta_1(0) = 1.001$, $\eta_0(0) = 0.999$, and $\beta_{10}(0) = 1.499$. (b) The dynamics with $\Delta\beta = 5.0$ and initial condition $\eta_1(0) = 1.2$, $\eta_0(0) = 0.9$, $\beta_{10}(0) = 5.05$. The solid, dashed and dotted lines represent $\eta_1(z)$, $\eta_0(z)$, and $\beta_{10}(z)$, respectively.

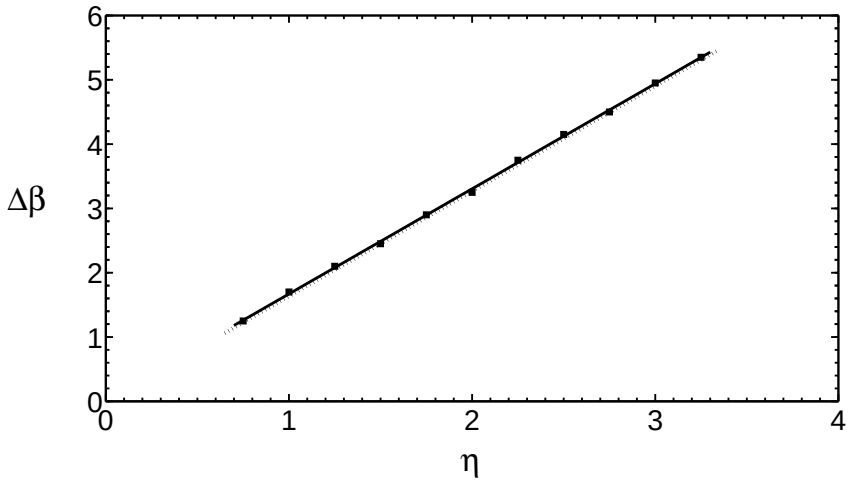

FIG. 12: The bifurcation diagram for the two-channel system perturbed by the Raman XFS. The squares correspond to the bifurcation values obtained by numerical solution of Eq. (33), while the solid line is a fit of the form $\Delta\beta_{bif} = 0.04 + 1.64\eta$ for the numerical data. The dotted line is the prediction of linear stability analysis: $\Delta\beta_{bif} \simeq 1.63\eta$.